Journal of Materials Chemistry C

ROYAL SOCIETY OF CHEMISTRY

PAPER

Published on 14 July 2026

Cite this: DOI: 10.1039/d6tc01728b

Immobilization of glucose oxidase and catalase on magnetite nanoparticles as functional catalyst supports

Angeles Valls-Chiva,†[abcd] Felipe Hornos,†*[e] Jose L. Hueso,[abcdf] Ana Martín-Pardillos[acdg] and Jesus Santamaria*[abcd]

Received 27th May 2026,
Accepted 11th July 2026

DOI: 10.1039/d6tc01728b

rsc.li/materials-c

In this work, we have prepared magnetite nanoparticles (MNPs) coated with polyethylenimine (PEI) to obtain a positively charged surface and showed their suitability as functional supports to successfully immobilize glucose oxidase (GOx) and catalase (CAT) enzymes. We have compared two immobilization strategies, namely electrostatic binding and covalent attachment mediated by glutaraldehyde cross-linking. To quantify the amount of immobilized enzyme (q_{max}), we have developed a methodological approach that minimizes the dependence of the q_{max} value on the equilibrium constant of the adsorption process (K). Catalytic studies showed high retention of enzymatic activity (100% for covalent binding and 75% for electrostatic binding), indicating that the immobilization protocol preserves the native conformation of the enzyme. Furthermore, the covalent strategy demonstrated stable binding even when the nanohybrid was subjected to extreme conditions (pH 3), retaining 91% of the enzyme on the surface, compared to 6% when immobilized electrostatically. These results highlight the importance of surface engineering in the design of magnetic biocatalysts for potential application in starvation or oxygen generation therapies.

Introduction

Cancer remains one of the leading causes of death worldwide and continues to pose major challenges due to heterogeneity among patients and across tumour types.[1] Current treatments still face limitations such as insufficient therapeutic efficacy, adverse side effects arising from the toxicity of the agents employed, and disease recurrence. Nanocatalytic medicine is emerging as a promising alternative for cancer therapy and a plethora of both inorganic and hybrid catalytic materials have been tested, attempting to alter the tumour microenvironment (TME) to create conditions that are less favorable for tumor growth.[2–12] In this regard, enzymes are central to biological function and offer catalytic efficiency and substrate selectivity.[2,9,11–19] Unlike broad-spectrum chemotherapeutic agents, enzymes act with high precision, recognizing specific molecular substrates under moderate physiological conditions.[20,21] Glucose oxidase (GOx) in particular has been proposed to enable starvation therapy by consuming the glucose required for tumour cell metabolism.[2,9,17,22–27]

Specifically, cancer cells rely on an accelerated glycolytic pathway to obtain energy, consuming much more glucose than healthy cells, a process known as the Warburg effect.[28,29] On the other hand, catalase (CAT) can be an excellent catalytic asset to convert hydrogen peroxide (H_2O_2) into oxygen (O_2) that is typically scarce in hypoxic tumour domains. A higher O_2 concentration would increase GOx enzymatic response and also the effectiveness of alternative cancer treatments, such as chemodynamic and photodynamic therapy, which are O_2-dependent.[22,30–32] However, therapeutic applications of free enzymes are often hindered by limited stability, off-target distribution and poor retention in the TME.[2,11] Furthermore, free proteins are susceptible to proteolytic degradation and rapid systemic clearance, which drastically reduces their biological half-life.[33] On the other hand, inorganic enzyme-mimicking surrogates are promising and widely explored, but also present major challenges such as limited specificity, potential toxicity, the need for clearance after

[a] Instituto de Nanociencia y Materiales de Aragon (INMA) CSIC-Universidad de Zaragoza, Campus Rio Ebro, Edificio I + D, C/Poeta Mariano Esquillor, s/n, 50018, Zaragoza, Spain. E-mail: jesus.santamaria@unizar.es
[b] Department of Chemical and Environmental Engineering, University of Zaragoza, Campus Rio Ebro, C/María de Luna, 3, 50018 Zaragoza, Spain
[c] Networking Research Center on Bioengineering, Biomaterials and Nanomedicine (CIBER-BBN), 28029, Madrid, Spain
[d] Instituto de Investigación Sanitaria (IIS) de Aragón, Avenida San Juan Bosco, 13, 50009 Zaragoza, Spain
[e] Instituto de Investigación en Biotecnología y Salud (IDiBE), Universidad Miguel Hernández, 03202 Elche, Spain. E-mail: fhornos@umh.es
[f] Escuela Politécnica Superior, U. Zaragoza, Crta. de Cuarte s/n, 22071, Huesca, Spain
[g] Departamento de Bioquímica y Biología Molecular y Celular, Facultad de Ciencias de la Salud y del Deporte, Campus de Huesca, U. Zaragoza, Spain
† Equal contribution.

completing their function, frequent instability in biological environments, challenges in control and regulation, and possible induction of immune responses.[11] As an alternative, the immobilization of natural enzymes onto solid supports can enhance robustness and provide a hybrid catalyst with high selectivity and biocompatibility. Nevertheless, enzyme–surface interactions are also challenged by non-specific adsorption events that perturb conformational integrity, promote aggregation, and ultimately compromise function.[13–16]

In this work, we present the use of magnetite nanoparticles (Fe_3O_4 NPs, hereafter MNPs) as solid supports and different functionalization strategies to validate the effective immobilization of GOx and CAT. For this immobilization, selecting a suitable interface is essential. We have chosen polyethylenimine (PEI), a branched cationic polymer known for its high density of primary, secondary, and tertiary amines. PEI serves a dual purpose: it stabilizes the MNPs at physiological pH, prevents direct contact between the enzyme and the rigid inorganic core, and provides a versatile chemical binding site for electrostatic or covalent anchoring (both strategies are widely used in the field of enzyme immobilization).[34–36] MNPs have already been tested as highly biocompatible nanomaterials with theranostic capabilities and well-known surface chemistry.[13,17,25,37,38] Although some works have explored immobilization of these enzymes on magnetic supports,[39–47] the literature still lacks a systematic evaluation of this system. In this work we include the use of different molecular weights of PEI, different types of binding, electrostatic *versus* covalent, and a study of the colloidal stability of the nanohybrid with different amounts of supported enzyme. In addition, a rigorous method for determining the maximum enzyme immobilization capacity (q_{max}), is provided. Our goal is to provide a comprehensive guide for optimizing the catalytic activity and stability of such magnetic nanohybrids intended for advanced biomedical applications.

Experimental

Synthesis of magnetite nanoparticles (MNPs)

MNPs (Fe_3O_4) were synthesised following a chemical co-precipitation protocol from iron salts of >99% purity following the method proposed by Massart.[48] $FeCl_2{\cdot}4H_2O$ (198.83 g mol^{-1}) and $FeCl_3{\cdot}6H_2O$ (273.3 g mol^{-1}) were purchased from Merck, and all other reagents (ammonia, acids, *etc.*) were obtained from Thermo Fisher and Sigma-Aldrich. Briefly, 32.80 g of $FeCl_3{\cdot}6H_2O$ and 12.06 g of $FeCl_2{\cdot}4H_2O$ were dissolved in 1 L of deionised water under a nitrogen flow. A 25 wt% ammonia solution was added dropwise while monitoring the pH until it reached approximately 10, and the mixture was then stirred for 1 h at this pH. The solution immediately turned black, indicating the formation of magnetite. The dispersion was then heated to 70 °C and stirred for an additional 1 h under an N_2 atmosphere. After this period, the suspension was stirred overnight at room temperature without the nitrogen flow. The pH was then adjusted to 7, and the particles were washed three times with Milli-Q water, using 1.3 T neodymium magnets to retain the MNPs and remove excess ammonia. Finally, the MNPs were stored as aliquots at 4 °C. The synthesis and characterization of materials were performed by the Platform of Production of Biomaterials and Nanoparticles of the NANBIOSIS ICTS, more specifically by the Nanoparticle Synthesis Unit (Unit 9) of the CIBER in Bioengineering, Biomaterials & Nanomedicine (CIBER-BBN).

Coating of MNPs with poly(ethyleneimine) (PEI)

The polyelectrolyte used to coat the MNPs and provide a positive surface charge was polyethylenimine (PEI);[49] the monomer structure and key characteristics are summarized in Table 1. PEI samples of different molecular weights (60 000 Da and 25 000 Da) were purchased from Sigma-Merck. MNPs were sonicated using a UW 2200 ultrasonic probe (Bandelin Sonoplus) for 5 min with intermittent pulses (10 s on, 10 s off) at 40% amplitude. Subsequently, the MNP suspension (0.36 mg mL^{-1}, 16 mL) was added dropwise to a PEI solution at pH 7 (7.2 mg mL^{-1}, 500 mL) at a 1 : 20 (w/w) MNP:PEI ratio (this procedure was carried out using PEI with molecular weights of 60 000 Da and 25 000 Da, respectively), at room temperature under stirring overnight. The MNPs were then precipitated with sodium dihydrogen phosphate (NaH_2PO_4; 500 mM; pH 7) and washed thrice with water by centrifugation to remove excess free PEI and phosphates.

Selection of enzymes, main features and quantification methodology

Two enzymes were used in this work: glucose oxidase (GOx) and catalase (CAT). Their structures and selected relevant properties are described in Tables 2 and 3.

Determination of the enzyme concentration by spectrophotometry

To determine the concentrations of GOx and CAT, their absorbance at 280 nm was measured, since at this wavelength aromatic amino acids such as tryptophan, tyrosine, and phenylalanine absorb light. Using the measured absorbance (A) and the Lambert–Beer law ($A = \varepsilon{\cdot}b{\cdot}c$), where ε is the molar extinction coefficient characteristic of each enzyme, b is the optical path length of the cuvette, and c is the concentration of the analyte, the concentrations of GOx and CAT were obtained using the molar extinction coefficients listed in Tables 2 and 3.

Table 1 Polyethylenimine features

Polyethylenimine (PEI)	
Molecular formula (monomer)	C_2H_4N
Molecular weight (monomer)	42.05 g mol^{-1}
Chemical structure	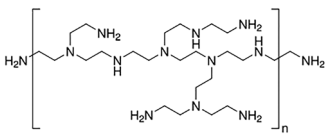

Table 2 Glucose oxidase main features

Characteristics of glucose oxidase (GOx)	
Origin	*Aspergillus niger*
CAS number	9001-37-0
Supplier	Sigma-Aldrich
Optimal pH	5.5–6.0
Molecular weight	65 kDa (per subunit)
Isoelectric point	5.02
ε_{280} (molar extinction coefficient)	1.475 (mg mL^{-1})$^{-1}$ cm^{-1}
Three-dimensional structure (Uniprot)	

Determination of the amount of immobilized enzyme (q_{max})

The maximum capacity of a nanoparticle (NP) to bind a given enzyme (q_{max}) is key in NP functionalization with enzymes, where the aim is to optimize the amount of enzyme that can be attached while maximizing catalytic activity or overall system functionality.

q_{max} can be affected by factors such as the NP size and shape, surface properties and charge, and the conditions of the medium. Herein, q_{max} was determined experimentally by adsorption experiments that were fitted to a Langmuir isotherm model. Although developed for gas–solid systems, the Langmuir model is frequently used to explain the adsorption of other ligands – particularly proteins/enzymes – in sufficiently dilute suspensions. In this case, a Type I (Langmuir) isotherm (eqn (1)) was used:

$$q = \frac{m_{prot}}{m_{NP}} = \frac{K \cdot [P]}{1 + K \cdot [P]} \cdot q_{max} = \frac{[P]}{K_D + [P]} \cdot q_{max} \quad (1)$$

where q is the mass of the enzyme adsorbed per unit mass of NPs, q_{max} is the maximum amount of enzyme immobilized per unit mass of NPs (at saturation), [P] is the enzyme concentration in solution, and K is the equilibrium constant of the adsorption process ($K_D = 1/K$ is the dissociation constant).

Table 3 Catalase main features

Characteristics of catalase (CAT)	
Origin	*Bos taurus* (liver)
CAS number	9001-05-2
Supplier	Sigma-Aldrich
Optimal pH	7.0
Molecular weight	250 kDa (59.9 kDa per subunit)
Isoelectric point	5.4
ε_{280} (molar extinction coefficient)	3.65 (mg mL^{-1})$^{-1}$ cm^{-1}
Three-dimensional structure (Uniprot)	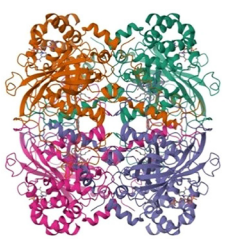

For a constant NP concentration, q increases in a saturable manner with [P]. As [P] increases, the increment in q becomes progressively smaller, approaching q_{max} when the NP surface is fully covered with protein.[50]

As mentioned above, there are several well-established isotherm models, including the Brunauer–Emmett–Teller (BET), Freundlich, and Temkin models, among others.[51] Since our goal is not to determine whether the enzyme follows one model or another in terms of the immobilization process, but rather to obtain a quantifiable value (q_{max}) that allows us to compare different conditions in that process, we have chosen to use the Langmuir isotherm. From the Langmuir isotherm, information can be obtained on both the adsorption affinity (equilibrium constant K) and the maximum adsorption capacity (q_{max}). The Langmuir model describes the situation in which protein P (enzyme) in solution is in equilibrium with that adsorbed on the surface S:

$$S + P \rightleftharpoons S{\cdot}P$$

In many cases (as is the case with our study), the parameter of interest is the maximum adsorption capacity of protein P (enzyme) per particle, q_{max}. While typically this would be obtained in experiments where the amount of enzyme adsorbed on the NPs would be measured using a fixed amount of NPs and increasing enzyme concentrations until a plateau of enzyme adsorbed was reached, in this work we have used an alternative approach involving the use of increasing concentrations of NPs but under a fixed, high concentration of enzyme ([P] $\gg K_D$), in such a way that the nanoparticles are permanently saturated with the enzyme. Under these conditions, if [P] $\gg K_D$:

$$q = \frac{m_{prot}}{m_{NP}} = \frac{[P]}{K_D + [P]} \cdot q_{max} \approx \frac{[P]}{[P]} \cdot q_{max} = q_{max} \quad (2)$$

Thus,

$$(m_{prot})_{adsorbed} = q_{max} \cdot m_{NP} \quad (3)$$

where m_{NP} is the mass of the NPs present in the dispersion. Since the total protein mass in the sample is known,

$$(m_{prot})_{total} = (m_{prot})_{adsorbed} + (m_{prot})_{dissolution} \quad (4)$$

Rearranging and replacing gives:

$$(m_{prot})_{dissolution} = (m_{prot})_{total} - q_{max} \cdot m_{NP} \quad (5)$$

Dividing by the sample volume:

$$[P]_{dissolution} = [P]_{total} - q_{max} \cdot [NP] \quad (6)$$

Therefore, if a series of samples is prepared in which the total protein concentration, $[P]_{total}$, is kept approximately constant at a high value ([P] $\gg K_D$), in the presence of increasing NP concentrations, a plot of the remaining concentration of free protein in solution should decrease linearly with NP concentration (eqn (6)). In this case, the slope of the resulting straight line is equal to

$-q_{max}$, and the amount of enzyme on the NPs can be obtained with very good accuracy.

Electrostatic immobilization of enzymes and evaluation of stability

To determine the maximum amount of enzyme (q_{max}) that could be immobilized on our MNPs, increasing concentrations of MNPs (0–0.08 mg mL^{-1}) were incubated while keeping the GOx concentration constant (0.5 mg mL^{-1}) for all solutions and adjusting the pH to 7 using 10 mM HEPES buffer. The dispersions were stirred overnight at 37 °C. After incubation, the samples were centrifuged and the supernatants were analyzed by UV-Vis spectroscopy to determine the remaining enzyme concentration. q_{max} values were determined for MNPs coated with PEI-60 kDa and with PEI-25 kDa. In addition, this study was performed both without ionic-strength supplementation and in the presence of ionic strength (150 mM). The stability of the system was also assessed by lowering the pH to 3 after enzyme immobilization. To evaluate the stability of the electrostatic interaction, the system was challenged by adjusting the pH to 3 and incubating under stirring at 37 °C overnight. Samples were then centrifuged for 20 min at 13 000*g*. The supernatant was collected to determine the concentration of any enzyme released using a UV/Vis V-67 spectrophotometer (JASCO; Madrid, Spain), and the catalytic activity of the pellet was measured (Scheme 1).

Covalent immobilization of GOx or CAT *via* glutaraldehyde and evaluation of the stability

MNPs@PEI were activated by incubation with glutaraldehyde (GA) at 5% (v/v) in Milli-Q water at room temperature overnight. In this approach, a linkage is formed between the amine groups of PEI and one of the aldehyde groups of GA. Simultaneously, the second aldehyde group of GA, which remains exposed to the medium, reacts with amino groups on the enzyme to form an imine (Schiff base), thereby ensuring covalent attachment.[13,15,52]

In the same way as for adsorption-based anchoring, q_{max} was determined for covalent immobilisation; however, in this case it was measured for MNPs@PEI previously activated with 5% (v/v) GA, rather than for MNPs@PEI. q_{max} values were determined separately for glucose oxidase (GOx) and catalase (CAT). Increasing concentrations of activated MNPs@PEI were used, from 0 to 0.234 mg mL^{-1} for GOx and from 0 to 0.254 mg mL^{-1} for CAT, while fixing the GOx concentration at 0.30 mg mL^{-1} and the CAT concentration at 0.15 mg mL^{-1}, respectively. The suspensions were stirred overnight at 37 °C and, after incubation, the samples were centrifuged, and the enzyme concentration in the supernatants was measured by UV-Vis spectroscopy. The stability of the covalent linkage was again assessed by subjecting the system to pH 3 under stirring at 37 °C overnight. Samples were then centrifuged for 20 min at 13 000*g*. The supernatant was collected to determine the enzyme concentration using a UV/Visible V-67 spectrophotometer (JASCO; Madrid, Spain), and the catalytic activity of the pellet was measured.

Colloidal stability of MNPs@GOx as a function of % q_{max}

To study the colloidal stability of the different nanohybrids as a function of q_{max}, the hydrodynamic size of the MNPs25@GOx-C system was evaluated as a function of enzyme loading in aqueous solution (Milli-Q water). In addition, the zeta potential was determined. For this purpose, a fixed concentration of MNPs25 (0.1 mg mL^{-1}), previously activated with GA, was incubated with different percentages of GOx q_{max}, ranging from 10% to 100%. The samples were incubated overnight at room temperature under agitation, and the following day their hydrodynamic size was measured by dynamic light scattering (DLS) and their zeta potential by electrophoretic light scattering (ELS), using a 90Plus instrument (Brookhaven Instruments Corporation). For electrostatic immobilization, the same procedure was followed, but the pH was adjusted to 7.0 using HEPES buffer.

Evaluation of the catalytic activity of the MNPs-GOx: Indirect quantification of GOx activity: O_2 consumption measurements

The dissolved O_2 concentration was measured with a NeoFox oximeter equipped with a FOSPOR-R probe. To study O_2 consumption, the MNPs@PEI@GOx system was incubated with 1000 ppm glucose in 10 mM HEPES buffer. Free enzyme was used as the positive control and MNPs@PEI as the negative control.

Evaluation of the catalytic activity of the MNPs-GOx in a hypoxic environment

O_2 is an essential and limiting reactant in the GOx-catalyzed reaction.[27] Its solubility varies with the medium: in pure water

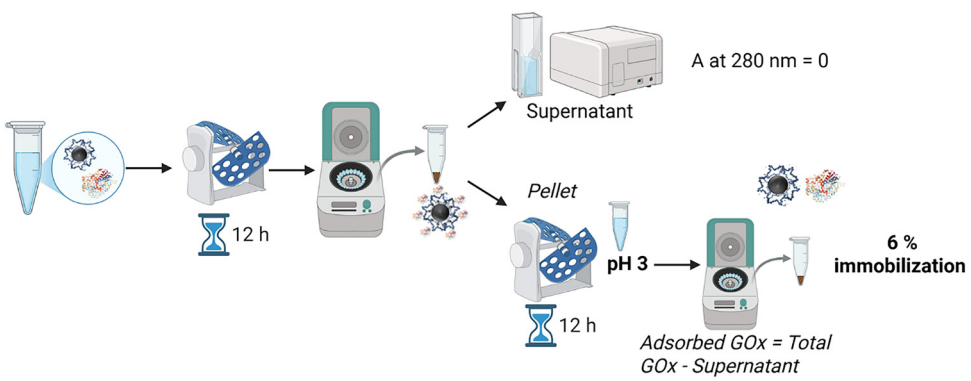

Scheme 1 Schematic representation of the desorption study in the electrostatic adsorption-based immobilization.

at 25 °C it is approximately 9 mg L^{-1};[53] in cell culture media equilibrated in air it is between 6 and 11 mg L^{-1};[54] and in human arterial blood only a small fraction of O_2 is in plasma (approximately 6.4 mg L^{-1}), while the majority (98.5%) is bound to hemoglobin within red blood cells. Therefore, catalysis under an inert atmosphere (hypoxic conditions) was performed.[55] In a three-necked flask, nitrogen was bubbled through the solution for 30 min to displace dissolved O_2. O_2 was then added until a concentration of 1 ppm was reached, as quantified using the NeoFox oximeter, and glucose quantification was performed simultaneously using the glucometer.

Evaluation of the catalytic activity of the MNPs-CAT: direct quantification of CAT activity: O_2 generation measurements

The dissolved O_2 concentration was measured with a NeoFox oximeter equipped with a FOSPOR-R probe. To study O_2 generation, the MNPs@PEI@CAT system was incubated with 1 mM H_2O_2 in 10 mM HEPES buffer. Free enzyme was used as the positive control and MNPs@PEI as the negative control.

Characterization techniques

Quantification by MP-AES. The Fe concentration was measured using an MP-AES 4100 instrument (Agilent; Madrid, Spain), operated with MP Expert software and equipped with a magnetically excited microwave plasma source and a wide-range charge-coupled device (CCD) detector. MP-AES is based on the excitation of atoms in a nitrogen microwave plasma and the subsequent detection of their characteristic atomic emission wavelengths, enabling accurate elemental quantification. Prior to analysis, samples were digested in aqua regia ($HCl:HNO_3$, 3 : 1) to ensure complete dissolution of the iron-containing materials and subsequently diluted until the iron concentration fell within the calibration range (1–40 ppm).

Dynamic light scattering (DLS) and zeta potential measurements. Hydrodynamic diameter and zeta potential measurements were performed using a Zetasizer Nano instrument (Malvern Instruments, UK) or a Brookhaven 90Plus analyzer. Samples were dispersed in an aqueous medium and analyzed at room temperature. A titration study of size and zeta potential as a function of the GOx loading capacity on the nanoparticles (MNPs@PEI), both activated and non-activated, was also carried out. These measurements were used to evaluate the colloidal stability of the nanoparticles and to monitor changes in particle size and surface charge after the different functionalization steps.

Transmission electron microscopy (TEM). The morphology and particle size distribution of the nanoparticles, both uncoated and coated, were determined by transmission electron microscopy (TEM) using a Tecnai T20 system (Thermo Fisher; Hillsboro, OR, USA) operated at 200 kV, with a resolution of up to 0.24 nm. TEM samples were prepared by dispersing the sample in water and drop-casting 5 μL onto a 200-mesh holey carbon grid (Electron Microscopy Sciences; Hatfield, PA, USA), followed by air-drying using anti-capillary tweezers. Particle size distributions were obtained by measuring at least 50 individual nanoparticles from representative TEM micrographs using ImageJ software.

X-ray photoelectron spectroscopy (XPS) and X-ray diffraction (XRD). The elemental composition and oxidation states of surface elements were determined by X-ray photoelectron spectroscopy (XPS) using a Kratos Tech AXIS Supra spectrometer. The samples were attached to a sample rod within the pretreatment chamber of the spectrometer and subsequently evacuated at room temperature. The spectra were acquired using monochromatic Al Kα radiation (120 W) at 8 mA and 15 kV, with a pass energy of 20 eV. Binding energies were referenced to the internal C 1s standard (284.5 eV). Peak fitting was performed using CasaXPS software, applying a weighted sum of Lorentzian and Gaussian component curves after Shirley background subtraction. The crystal structure and phase composition of the NPs were analyzed by X-ray diffraction (XRD) using a PANalytical Empyrean instrument equipped with a PIXcel1D detector and Cu Kα radiation. Data were collected over 5–89.98° with a step size of 0.0130°.

Results and discussion

Stabilization of MNPs with PEI and characterization at physiological pH

We synthesized MNPs by precipitation of iron salts.[48] X-ray diffraction confirmed the sole presence of the cubic spinel magnetite crystalline phase (Fig. 1a). TEM analysis confirmed the presence of pseudo-spherical nanoparticles with a primary particle size of 15 ± 3 nm (Fig. 1b). We coated them with poly(ethyleneimine) (PEI) to provide a positive charge that enhances their colloidal stability at physiological pH and facilitates the subsequent immobilization of the enzymes.[14,49,52,56] Two different PEI molecular weights of 60 and 25 kDa were tested (yielding hybrids termed MNPs60 and MNPs25). As can be seen in Fig. 1c and d, the primary particle size did not vary significantly after the PEI coating processes.

Since uncoated NPs were unstable at physiological pH and have no surface charge,[57] their size and charge were measured at pH 11. DLS analysis revealed increasing hydrodynamic sizes from 37 nm, for uncoated MNPs, up to 230 nm in the presence of higher MW branched PEI, indicating some formation of aggregates (Table 4). Upon coating with PEI, the net charge (ζ-potential) of the MNPs switched from −53 mV ± 4 mV to positive values above +20 mV in HEPES at physiological pH, thereby confirming the successful coating of the MNPs with the branched PEIs of 60 and 25 kDa, respectively (Table 4). The final sizes suggest the embedding of several NPs within the polyelectrolyte network. This phenomenon is not necessarily detrimental and is, in fact, common in systems where nanoparticles are assembled *via* layer-by-layer techniques, leading to structures in which nanoparticles are distributed along the polymeric chains.[13–16,52,56,58,59]

XPS corroborated the co-existence of both Fe^{2+}/Fe^{3+} valence states and the presence of different amine surface moieties (Fig. 2). The fitted Fe 2p spectrum (Fig. 2a) shows mixed Fe^{2+}/Fe^{3+} states, with the Fe $2p_{3/2}$ peak at ∼710.6 eV (Fe^{2+}: 15.9 at%, Fe^{3+}: 31.2 at%) and the Fe $2p_{1/2}$ peak at ∼724 eV (Fe^{2+}: 8.0 at%, Fe^{3+}: 15.7 at%), together with their characteristic satellite peaks. The spectrum of O1s (Fig. 2b) exhibits two contributions

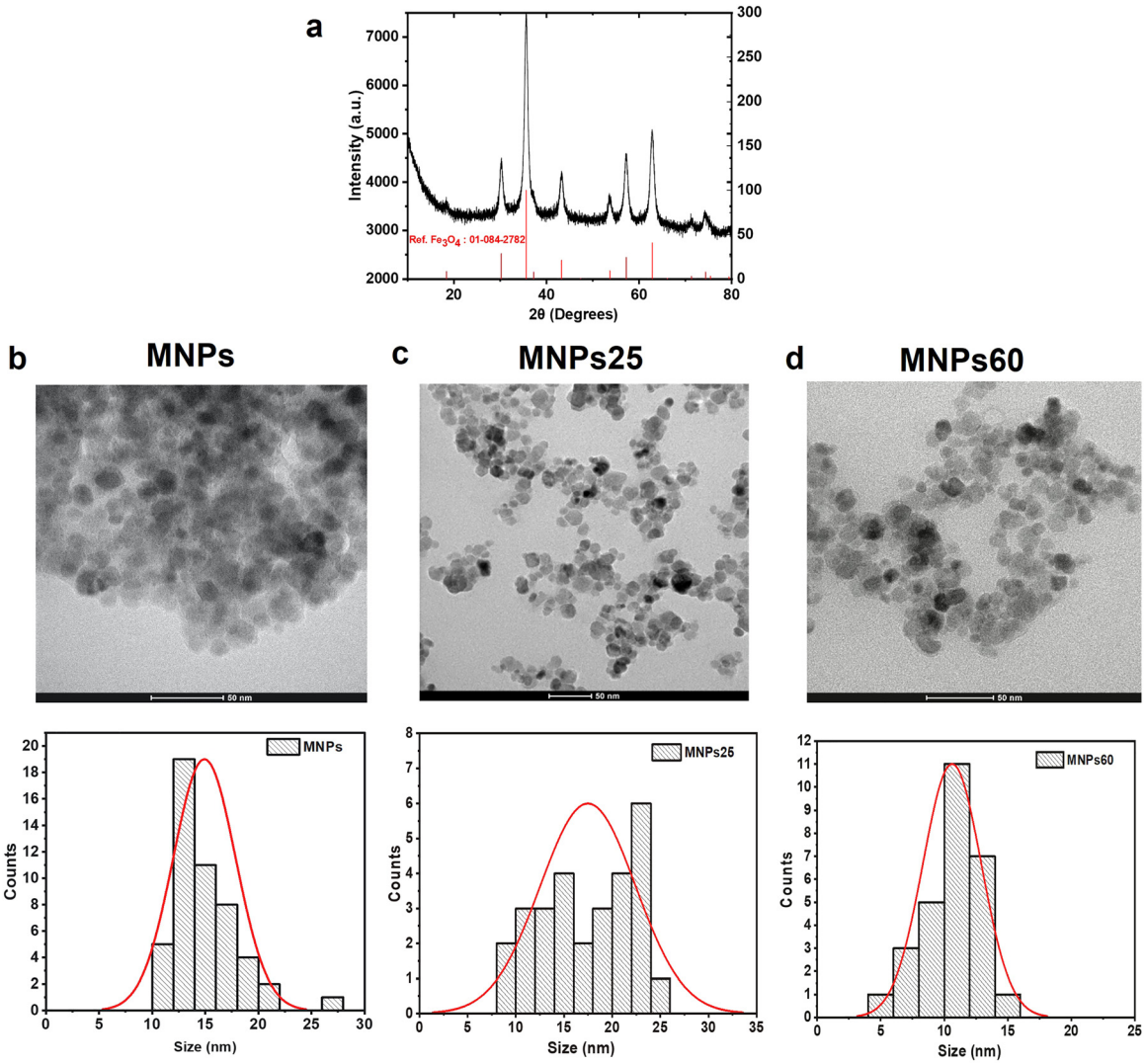

Fig. 1 (a) X-ray diffractogram showing a good match with the cubic spinel Fe_3O_4 structure. Particle size distribution determined by TEM (n = 50) of (b) uncoated magnetite nanoparticles, (c) after coating with PEI-25 kDa and (d) after coating with PEI-60 kDa. Scale bar: 50 nm.

attributed to different oxygen lattice (O^{2-}) coordination positions within the Fe–O structure and a secondary component at ~532 eV. The C1s, N1s regions and XP survey spectra validated the successful coating of the nanoparticles with PEI (Fig. 2c, d and Fig. S2).

Electrostatic immobilization of GOx on MNPs60 and MNPs25

In most studies, the amount of enzyme immobilized on the surface (q_{max}) is typically quantified by a single-point measurement, by calculating the concentration differences[60] in the supernatant before and after immobilization. Other studies calculate this value after immobilization, separating the enzyme from the surface and quantifying the concentration of the enzyme that was previously immobilized.[61] Here, we have used a different method, as explained in the experimental section, that operates under protein-saturating conditions ([P] ≫ K_D), *i.e.* with the existing NPs loaded with enzyme at maximum capacity. Thus, a decreasing linear relationship between the remaining free enzyme and the concentration of NPs is obtained (eqn (6)), as shown in Fig. 3b and c.

Table 4 Determination of hydrodynamic diameters (D_h) and ζ potential of uncoated MNPs (at pH 11.0, ammoniacal medium), MNPs60 and MNPs25 (HEPES 10 mM, pH 7.0)

Type of MNP	D_h (nm)	ζ potential (mV)
Uncoated MNPs	37 ± 5	−53 ± 4 (pH 11)
MNPs60	230 ± 15	+41 ± 2 (pH phys.)
MNPs25	75 ± 12	+25 ± 1 (pH phys.)

The first attempt at immobilization of GOx exploited the electrostatic interactions between the positively charged amino groups exposed by PEI and the GOx (isoelectric point ~5.02), which carries a negative charge at physiological pH (Fig. 3a). The maximum capacity of MNPs@PEI to immobilize GOx (q_{max}) was evaluated for both PEI samples as described in the Experimental section, monitoring the unbound enzyme concentration. The

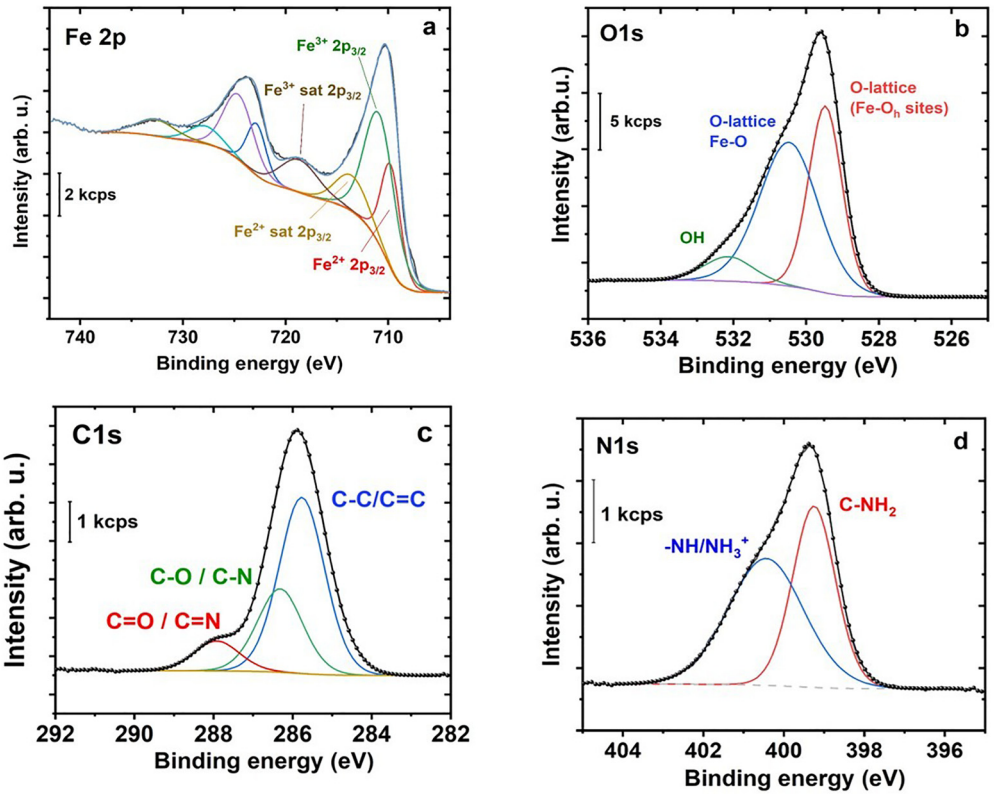

Fig. 2 X-ray photoemission spectra corresponding to the MNPs after coating with PEI-25 kDa: (a) fitted Fe 2p region (legends shown corresponding only to the $Fe2p_{3/2}$ region), (b) fitted O 1s region, (c) fitted C 1s region, and (d) fitted N 1s region.

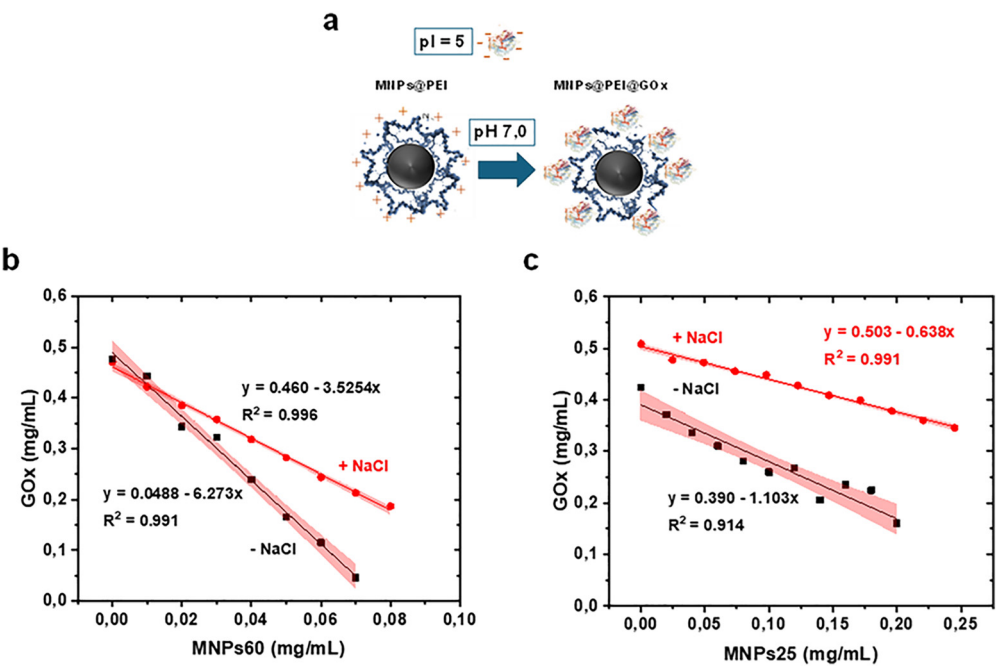

Fig. 3 (a) Schematic representation of the adsorption process of GOx onto MNPs-PEI (10 mM HEPES, pH 7.0); (b) variation of remaining free enzyme as a function of MNP60 concentration allows obtaining q_{max} of GOx in 10 mM HEPES buffer (pH 7.0), in the absence (black) or presence (red) of added ionic strength (150 mM NaCl). (c) Variation of remaining free enzyme as a function of MNP25 concentration allows obtaining q_{max} of GOx in 10 mM HEPES buffer (pH 7.0), in the absence (black) or presence (red) of added ionic strength (150 mM NaCl); panels (b) and (c) include the 95% confidence bands (shaded areas) of the linear fit.

MNPs60 loaded 6.3 ± 0.2 mg of GOx per mg of MNP in the absence of added ionic strength (10 mM HEPES, pH 7.0), and 3.52 ± 0.08 mg of GOx per mg of MNPs in the presence of an ionic strength of 150 mM (Fig. 3b). In this way, using this rigorous method, we can compare how surface functionalization affects enzyme immobilization. TEM images showed no significant differences after the enzyme was immobilized on MNPs60 (Fig. S1). In contrast, MNPs25 immobilized 1.1 ± 0.1 mg and 0.64 ± 0.02 mg of GOx under analogous conditions (Fig. 3c). These q_{max} values are comparable to those reported in the literature. For example, in the study by Ding *et al.*,[62] a q_{max} of 1.3 mg mg^{-1} was reported for NPs with high selectivity toward histidine-rich proteins. In the same study, much lower adsorption capacities were reported for other proteins, such as BSA (0.3 mg mg^{-1}) or lysozyme (0.2 mg mg^{-1}). Therefore, the values obtained here – particularly in the absence of ionic strength – are comparable to the best results reported, showing a high adsorption capacity, as discussed below (see also Table 5). Moreover, even under ionic strength conditions, the adsorption capacity remained higher than that of many studies presented in the literature.[57]

Colloidal stability of the GOX-MNPS-PEI system as a function of % q_{max}

Keeping in mind the potential application of these hybrids for nanocatalytic medicine, an aggregation-stability study was carried out in 10 mM HEPES, pH 7.0, at different loadings, measured as percentages of q_{max}. For this purpose, the concentration of the MNPs@GOx hybrids was fixed at 0.05 mg mL^{-1}, and both particle size and ζ-potential were measured by DLS, as shown in Fig. 4. As can be observed, between 0 and 40% of the maximum adsorption capacity (q_{max}), the size of the MNPs60@GOx system remained stable at approximately 250 nm. However, upon reaching 50% of q_{max}, the system became unstable and quickly aggregated (Fig. 4a). This behavior was consistent with zeta potential measurements: below 40% adsorption the system remained highly positively charged, whereas above this threshold the increasing amount of negatively charged GOx on the NP surface led to a progressive reduction in electrostatic repulsion, ultimately promoting aggregation (Fig. 4b). In the case of the MNPs25@GOx hybrid, it remained stable at approximately 100 nm. However, beyond 20% of q_{max}, the system became progressively unstable and formed increasingly larger aggregates (Fig. 4c). This behaviour correlated with zeta potential measurements: at low GOx contents ($\leq$20% of q_{max}), the NPs remained highly positively charged, while higher enzyme loadings led to a progressive reduction of surface charge due to the accumulation of negatively charged GOx, weakening electrostatic repulsion and promoting aggregation. Measurements above 40% of q_{max} were not performed, since NPs precipitated, rendering zeta potential and size measurements unreliable. Although the aggregation mechanism was not studied in detail, two processes appear to be mainly responsible. On one hand, an electrostatic charge screening effect occurs as enzyme loading increases, reducing electrostatic repulsion and favouring aggregation. This is particularly clear in MNPs25@GOx, where moving from 20 to 25% of q_{max} halved the zeta potential and tripled the aggregate size. On the other hand, a phenomenon known as protein bridging may also take place.[63] At this point, particle size increases, stability is lost, and aggregation occurs. In any case, the results suggested that to obtain a stable system loaded with GOx, the maximum loading should be kept around 20% of q_{max}, *i.e.*, 0.22 mg of GOx per mg of MNPs25, which still represents a meaningful value according to previously discussed studies (see Table 5).

In summary, although the binding capacity of MNPs60 was higher than that of MNPs25, the hydrodynamic sizes were also larger. From this point of view, MNPs25 would be a preferred support, providing sizes of around 100 nm up to 20% of q_{max} and still being capable of immobilizing 0.6 mg of GOx per mg of MNPs25 under physiological ionic strength conditions (150 mM). Thus, the MNPs60 were not characterized further and subsequent efforts were devoted to exploring the enzymatic activity provided by MNPs25 given their more suitable size and potential for biomedical applications.[64]

Table 5 Maximum capacity for immobilizing GOx and CAT enzymes (q_{max}) on other nanomaterials

Enzyme	Nanomaterial	Immobilization strategy	q_{max} (mg g^{-1})	Ref.
GOx	MNPs@PEI60	Adsorption	6300	This work
	MNPs@PEI60	Adsorption	3530 (150 mM NaCl)	This work
	MNPs@PEI25	Adsorption	1100	This work
	MNPs@PEI25	Adsorption	640 (150 mM NaCl)	This work
	MIL-125 3D (microporous crystalline of titanium dicarboxylate with cyclic octamers)	Adsorption	500 (pH 6)	71
	$CoFe_2O_4$/APTS and $CoFe_2O_4$	Adsorption	0.047–0.05	72
	MNPs@PEI25	Covalent	570	This work
	Florisil (magnesium silicate)	Covalent	0.75	73
	Fe_3O_4 (APTES-modified magnetic nanoparticles)	Covalent	23.91	74
CAT	MNPs@PEI25	Covalent	70	This work
	Florisil (magnesium silicate)	Covalent	0.6–5.2	75
	Chitosan beads	Covalent	25.7	76
	Reduced graphene oxide–Fe_3O_4 (rGO–Fe_3O_4)	Adsorption	312.5	77
	Acrylamide/chitosan cryogel modified	Adsorption	17.6	78
	Cibacron Blue F3GA-functionalized chitosan microspheres (CB-CS)	Adsorption	28.4	79

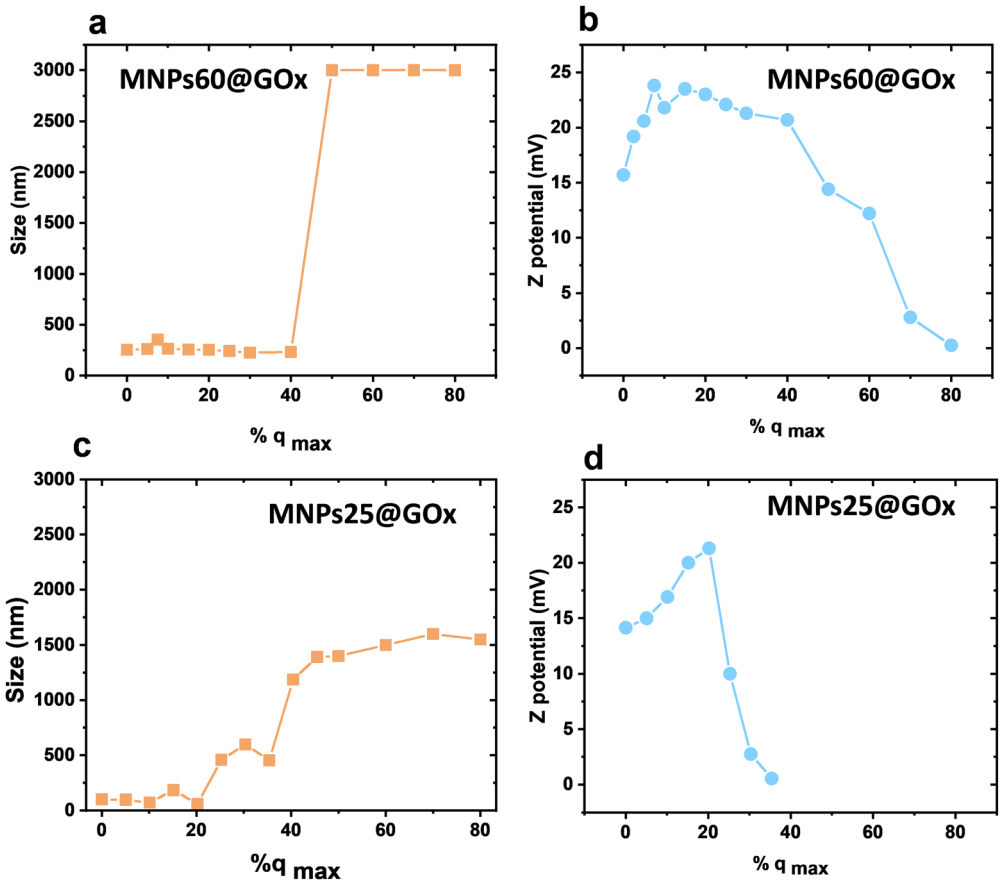

Fig. 4 Particle size and zeta potential of the MNPsPEI@GOx hybrids as a function of GOx loading in 10 mM HEPES buffer (pH 7.0): (a) hydrodynamic diameters of MNPs60@GOx; (b) zeta potential of MNPs60@GOx. (c) Hydrodynamic diameters of MNPs25@GOx and (d) zeta potential of MNPs25@GOx.

Electrostatic immobilization of GOx on MNPs25

Stability of the binding. To evaluate whether immobilization by adsorption had preserved the properties of the enzyme, catalytic activity was continuously monitored indirectly by measuring O_2 consumption as a consequence of glucose oxidation (see the Experimental section for details). The decrease was compared with an equivalent amount of free GOx (positive control at 0.001 mg mL^{-1}) and MNPs25 without GOx (negative control at 0.065 mg mL^{-1}). The hybrid MNPs25@GOx system was tested at a concentration of 0.065 mg mL^{-1} MNPs25 with the corresponding immobilized GOx enzyme, giving 0.001 mg mL^{-1} GOx (Fig. 5a and b). Both the positive control and the functionalized system exhibited a clear decrease in O_2 concentration. When using O_2 depletion as a measure of catalytic activity, it must be noted that this refers to dissolved O_2 that in a static (non-aerated) system is consumed much faster than it can be replenished from the gas phase. Then the system became mass-transfer limited, leading to a decrease in the slope (Fig. 5a). In view of this, the kinetic study was limited to the linear region of the slopes at short times ($t < 100$ s), where the decrease in the reaction rate due to mass transfer limitations is still negligible. When the slopes were compared (Fig. 5b) and normalized with respect to the kinetics obtained for free GOx, the system retained 75% of enzymatic activity after immobilization. These results again indicated that the adsorption of GOx onto MNPs25 did not compromise its catalytic efficiency, and that the orientation and accessibility of the enzyme's active site were not negatively affected upon immobilization. These findings are consistent with previous reports exhibiting high preservation of GOx catalytic activity upon immobilization onto magnetite NPs.[17,65] Regarding the structural integrity of immobilized enzymes, it is important to note that conventional biophysical characterization techniques, such as circular dichroism (CD) and intrinsic fluorescence spectroscopy, proved technically unfeasible in this system. Thus, strong light scattering in the far-UV range,[66] as well as light absorption across the entire UV-Vis spectrum,[67] cause complete masking of the protein signals. In fluorescence, the proximity of the magnetite NP induces a drastic quenching effect,[68] preventing a reliable conformational analysis of the protein.

In addition to the already discussed ionic strength experiments, binding stability assays were performed by lowering the pH to 3 (a reasonable value, since the pH inside a lysosome can reach values down to 4).[69] This challenge led to a significant GOx detachment (see Scheme 1 in the Experimental section). For MNPs25@GOx, electrostatic forces may be insufficient to retain the enzyme when confronted with extreme conditions of

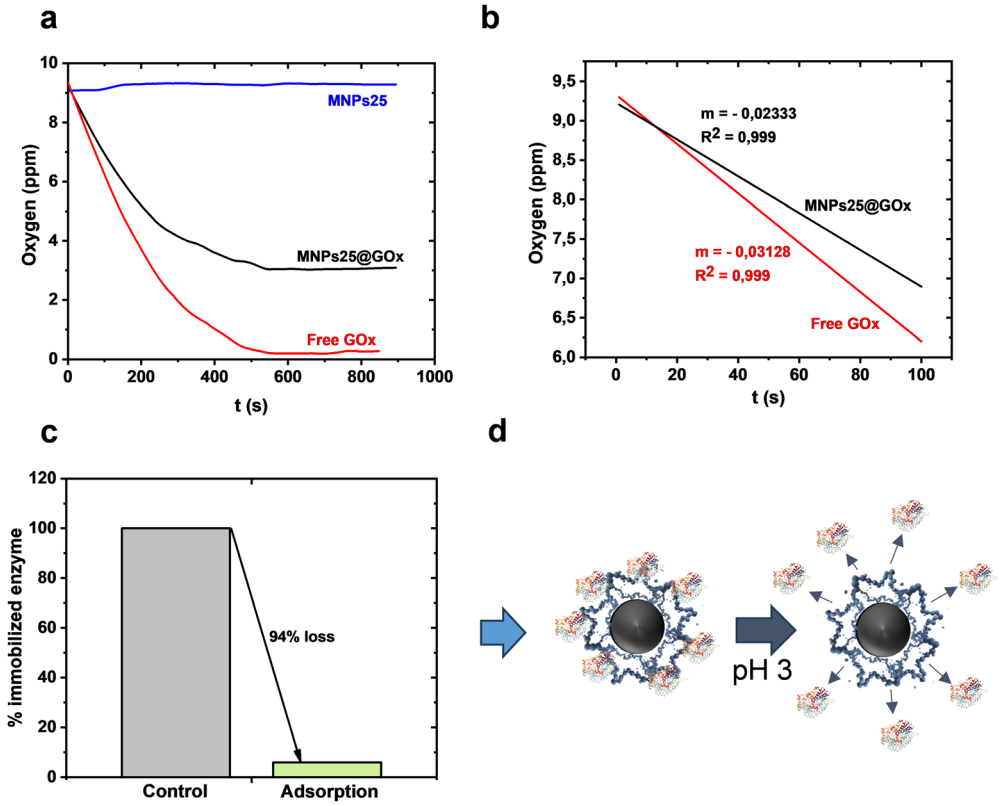

Fig. 5 (a) Catalysis by the MNPs25@Gox (black), the positive control, free GOx (red), and the negative control, MNPs25 (blue). Incubation with 1000 ppm glucose in PBS (pH 7.0); (b) initial slopes of the oxygen depletion curves for free GOx (red), and the MNPs25@GOx system (black). (c) Amount of enzyme retained on the surface after the pH change (from 7.0 to 3.0). The enzyme immobilized at pH 7 on MNPs25 (control) is shown in yellow and the enzyme immobilized after incubation at pH 3 (both activities were measured at pH 7.0 in PBS buffer) is shown in green. (d) Schematic representation of the GOx desorption process from MNPs-PEI (pH 3.0).

ionic strength or pH. Thus, when the pH was adjusted to 3.0, GOx desorbed almost completely, with only 6% remaining loaded on the MNPs (Fig. 5c and d). In addition, while the positive surface charge of MNPs25 enabled GOx immobilization, it would work the same for any negatively charged biomolecule, *i.e.*, for instance, plasma proteins, such as opsonins (opsonization process).[70] Competition with these proteins could also lead to the displacement of GOx from the NP surface.

Covalent immobilization of GOx on MNPs25

Stability of the binding. In view of these limitations, and particularly the possibility of partial enzyme release under changes in ionic strength or pH, an alternative immobilization strategy was tested, using covalent bonding of GOx onto MNPs25. Covalent immobilization was carried out with the aid of glutaraldehyde (GA). As shown in Fig. 6a, from the slope of the linear plot, the maximum capacity was found to be 0.57 mg of GOx per mg of MNPs25 (0.57 ± 0.03), lower than that obtained by adsorption (1.10 mg of GOx per 1 mg of MNPs25). Although these results might suggest that covalent immobilization is less efficient in terms of q_{max}, the covalent strategy offers the key advantage of stabilizing the enzyme, with no risk of desorption under pH, ionic strength variations or even from other enzymes competing for the surface and displacing the enzyme of interest. Furthermore, the aggregation and stability studies carried out in different media by DLS proved to be much more promising than those obtained by electrostatic adsorption, since higher enzyme coverage could be achieved (up to 85–90% of q_{max}) while keeping good colloidal stability (Fig. 6b and c). Analysis of O_2 consumption rates (Fig. 6d and e), showed that almost 100% enzymatic activity was retained, with no substantial difference observed between MNPs25@GOx-C (C: covalent) and free GOx, therefore, just as in adsorption immobilization, these results indicated that the covalent immobilization of GOx onto MNPs25 did not compromise its catalytic efficiency, and that the orientation and accessibility of the enzyme's active site were not negatively affected upon immobilization. Unlike immobilization by adsorption, when the enzyme was covalently immobilized and the pH was lowered to 3 (after re-incubating the nanohybrid at pH 7.0), approximately 91% of the enzyme remained immobilized on the MNPs25 (Fig. 6f), in contrast to the 94% loss observed when immobilized *via* electrostatic interaction. This strategy was therefore more effective for retaining the enzyme following pH changes or in the presence of plasma proteins that might compete with GOx for the NP surface.

Covalent immobilization of CAT

Enzymatic activity. A major limitation for GOx-based starvation therapy is the scarcity of available O_2 in the hypoxic TME.

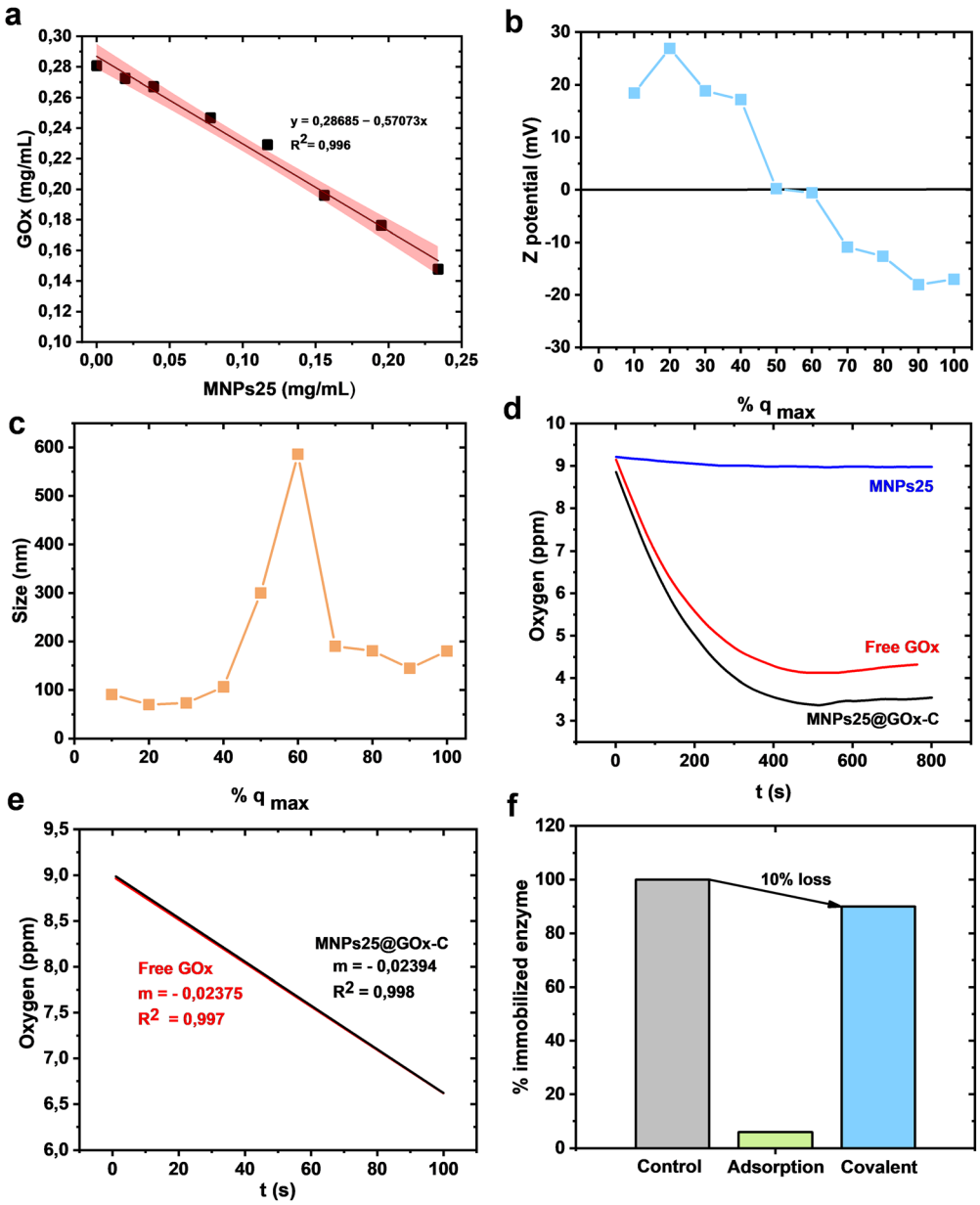

Fig. 6 (a) Determination of qmax of covalently immobilized GOx on MNPs25 (MNPs25@GOx-C). MNPs25 were activated with 5 wt% glutaraldehyde (GA) in aqueous solution and subsequently incubated with GOx (including the 95% confidence bands (shaded areas) of the linear fit); (b) zeta potential of the MNPs25@GOx-C bonded to different GOx loadings; (c) the corresponding hydrodynamic diameters measured in aqueous solution; (d) catalysis by MNPs25@GOx-C (black). The positive control, free GOx (red), and the negative control, MNPs25 (blue), are also shown. Incubation with 1000 ppm glucose in PBS (pH 7.0); (e) initial slopes of the oxygen depletion curves for free GOx (red) and the MNPs25@GOx system (black). (f) Amount of enzyme retained on the surface after the pH change (from 7.0 to 3.0). The enzyme immobilized at pH 7 on MNPs25 (control) is shown in yellow; the enzyme immobilized (adsorption) after incubation at pH 3 is shown in green; the enzyme immobilized (covalent) after incubation at pH 3 is shown in purple (all activities were measured at pH 7.0 in PBS buffer).

Indeed, Fig. 7a shows that MNPs25@GOx-C was unable to convert glucose under O_2 deprivation, while the addition of O_2 at the level of 2 ppm rapidly started the reaction. For this reason, we studied the incorporation of another enzyme capable of generating O_2 *in situ*, such as catalase (CAT), which decomposes H_2O_2 to release O_2. Covalent immobilization of CAT *via* GA was optimized using a similar procedure to GOx, to maximize the O_2 generation rate with the subsequent determination of q_{max} for CAT (Fig. 7b). The maximum capacity was found to be 0.07 ± 0.01 mg of CAT per 1 mg of MNPs25, approximately 8 times lower immobilization capacity than for GOx, which can be attributed to the difference in size between the two enzymes (Tables 2 and 3). Despite this, it exhibited significant catalytic activity upon H_2O_2 addition, as can be seen in Fig. 7c. Overall, the results of this work with GOx and CAT suggest that GA-mediated covalent bonding is an efficient strategy to immobilize therapeutic enzymes over MNPs coated with PEI.

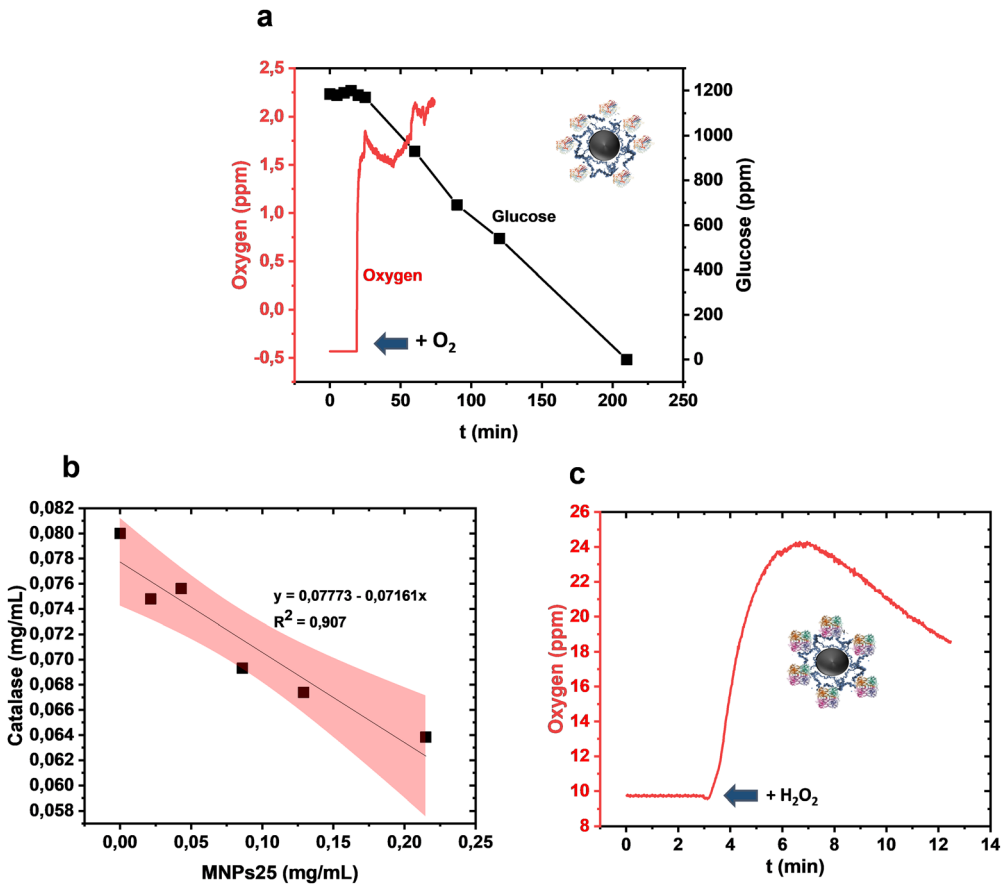

Fig. 7 (a) Activity of MNPs25@GOx-C under hypoxic conditions and its subsequent activation upon the addition of 2 ppm oxygen; (b) determination of q_{max} of covalently immobilized CAT on MNPs25 (MNPs25@CAT-C) (including the 95% confidence bands (shaded areas) of the linear fit). MNPs25 were activated with 5 wt% glutaraldehyde (GA) in aqueous solution and subsequently incubated with CAT; (c) evolution of oxygen concentration upon the addition of H_2O_2, under catalysis by MNPs25@CAT-C. All reactions were carried out in 10 mM HEPES buffer at pH 7.

Comparative analysis of maximum immobilization capacity (q_{max})

To better evaluate the maximum immobilization capacity (q_{max}) of the nanohybrids developed in this work, a comparative study was conducted against different NPs described in the literature for the immobilization of the same enzymes studied, GOx and CAT. Unfortunately, most of the NPs described in the literature as enzyme supports report immobilization under specific conditions only, and do not calculate the maximum enzyme immobilization capacity; in such cases, we have reported the data as found in different works (Table 5).

As can be seen from Table 5, the q_{max} values obtained in this study for GOx – both for electrostatic and covalent binding – are generally higher than those reported in the literature. In the case of CAT, few studies quantify covalent immobilization, but we still obtained immobilization capacity values considerably higher than those reported. For adsorption, reported values were generally lower than those reported in this work (with the exceptions summarized in Table 5).

Conclusions

We have developed a robust hybrid platform based on magnetite nanoparticles functionalized with polyethylenimine (PEI) that allows the effective immobilization of glucose oxidase (GOx) and catalase (CAT) and could also enable other functionalities (such as magnetic resonance imaging or hyperthermia), thanks to its magnetic core. Our systematic research demonstrates that critical parameters for the performance and optimization of the hybrid catalyst include the choice of PEI molecular weight and the mode of attachment of the enzyme on the NP surface (electrostatic *versus* covalent). While NPs stabilized by PEI with higher molecular weights exhibit greater enzyme immobilization capacity, it results in a convoluted structure where the final size of the nanohybrid increases considerably, which hinders applications in nanomedicine. On the other hand, covalent immobilization gives stable anchoring, allowing the retention of 91% of the enzyme bound after a low pH challenge, compared to 6% in the case of electrostatic immobilization. Furthermore, covalent immobilization preserves 100% of the activity, compared to 75% for electrostatic immobilization. For both electrostatic and covalent immobilization, a rigorous method has been followed to determine the maximum enzyme immobilization capacity (q_{max}), which is independent of the equilibrium constant. These magnetic nanohybrids with supported enzymes are attractive candidates for nanocatalytic medicine, particularly in starvation therapy and oxygen replacement strategies. This work provides the

physical and chemical foundation for the design of more complex multi-enzyme systems, in which both enzymes, GOx and CAT, could be immobilized simultaneously.

Author contributions

A. V. C.: methodology, data curation, formal analysis, validation, investigation, visualization, and writing – review and editing; F. H.: conceptualization, methodology, software, data curation, investigation, validation, formal analysis, supervision, visualization, writing – original draft, and writing – review and editing; J. L. H.: methodology, data curation, formal analysis, validation, investigation, visualization, writing – original draft, and writing – review and editing; A. M. P.: methodology, investigation, visualization, and writing – review and editing; J. S.: conceptualization, methodology, investigation, funding acquisition, project administration, supervision, resources, writing – review and editing, and writing – original draft.

Conflicts of interest

The authors declare no conflicts of interest.

Data availability

Data supporting the results published in this manuscript are available upon request from the corresponding author Dr Felipe Hornos, at the following address: fhornos@umh.es.

Supplementary information (SI): additional TEM images and XPS data. See DOI: https://doi.org/10.1039/d6tc01728b.

Acknowledgements

The authors acknowledge funding from the Spanish Research Agency (AEI) through the Plan Nacional project CONCERT (PID2023-148732NB-I00) and the Severo Ochoa Excellence Program (CEX2023-001286-S). J.S. also acknowledges the European Research Council (ERC) for funding the Advanced Grant Agreement Catalytic Dual-Function Devices Against Cancer (CADENCE-742684). F.H. acknowledges the Generalitat Valenciana and the European Social Fund for an APOSTD fellowship (APOSTD/2021/196) and the Conselleria de Innovación, Universidades, Ciencia y Sociedad Digital (CIAICO/2022/131). The study was also supported by the Aragon Government *via* the T57_23R research group. The synthesis and characterization of materials have been performed by the Platform of Production of Biomaterials and Nanoparticles of the NANBIOSIS ICTS, more specifically by the Nanoparticle Synthesis Unit (Unit 9) of the CIBER in Bioengineering, Biomaterials & Nanomedicine (CIBER-BBN). The authors acknowledge the use of instrumentation and technical support provided by the National Facility ELECMI ICTS, node 'Laboratorio de Microscopías Avanzadas (LMA)' at the Universidad de Zaragoza.

References

1 D. Hanahan, *Cancer Discovery*, 2022, **12**, 31–46.
2 B. Wang, N. Bao, L. Wang, J. Xiong, D. Li, Y. Wang, G. M. Ashraf and X. Wang, *Mater. Today Bio*, 2026, **36**, 102664.
3 L. Jiang, Z. Jin and Q. He, *Coord. Chem. Rev.*, 2025, **529**, 216430.
4 Z. Jin, L. Jiang and Q. He, *Nat. Commun.*, 2024, **15**, 3857.
5 B. Yang, Y. Chen and J. Shi, *Adv. Mater.*, 2019, **31**, 1901778.
6 J. I. Garcia-Peiro, M. Sancho-Albero, S. Miguel, A. Mosseri, F. Hornos, R. Contreras-Montoya, J. L. Hueso and J. Santamaria, *Adv. Funct. Mater.*, 2025, **35**, e02999.
7 J. I. Garcia-Peiro, J. Bonet-Aleta and J. L. Hueso, *Coord. Chem. Rev.*, 2025, **534**, 216542.
8 M. Encinas-Gimenez, A. Martín-Pardillos, J. Bonet-Aleta, E. Pérez, A. Rodríguez-Largo, J. L. Hueso, J. Santamaria and P. Martin-Duque, *Nanoscale*, 2025, **17**, 21614–21630.
9 Á. Valls-Chivas, J. Gómez, J. I. Garcia-Peiro, F. Hornos and J. L. Hueso, *Catalysts*, 2023, **13**, 980.
10 J. Bonet-Aleta, M. Encinas-Gimenez, E. Urriolabeitia, P. Martin-Duque, J. L. Hueso and J. Santamaria, *Chem. Sci.*, 2022, **13**, 8307–8320.
11 V. G. Panferov, X. Zhang, K.-Y. Wong, J. H. Lee and J. Liu, *Angew. Chem., Int. Ed.*, 2025, **64**, e202512409.
12 B. Torres-Herrero, I. Armenia, M. Alleva, L. Asín, S. Correa, C. Ortiz, Y. Fernández-Afonso, L. Gutiérrez, J. M. de la Fuente, L. Betancor and V. Grazú, *ACS Nano*, 2023, **17**, 12358–12373.
13 J. M. Bolivar, J. M. Woodley and R. Fernandez-Lafuente, *Chem. Soc. Rev.*, 2022, **51**, 6251–6290.
14 E. P. Cipolatti, A. Valério, R. O. Henriques, D. E. Moritz, J. L. Ninow, D. M. G. Freire, E. A. Manoel, R. Fernandez-Lafuente and D. de Oliveira, *RSC Adv.*, 2016, **6**, 104675–104692.
15 J. C. S. d Santos, O. Barbosa, C. Ortiz, A. Berenguer-Murcia, R. C. Rodrigues and R. Fernandez-Lafuente, *ChemCatChem*, 2015, **7**, 2413–2432.
16 C. Garcia-Galan, Á. Berenguer-Murcia, R. Fernandez-Lafuente and R. C. Rodrigues, *Adv. Synth. Catal.*, 2011, **353**, 2885–2904.
17 J. Huang, R. Zhao, H. Wang, W. Zhao and L. Ding, *Biotechnol. Lett.*, 2010, **32**, 817–821.
18 D.-M. Liu, J. Chen and Y.-P. Shi, *TrAC, Trends Anal. Chem.*, 2018, **102**, 332–342.
19 C. G. C. M. Netto, H. E. Toma and L. H. Andrade, *J. Mol. Catal. B: Enzym.*, 2013, **85–86**, 71–92.
20 Y. Pi, K. Ganabady and A. D. Celiz, *Commun. Mater.*, 2025, **6**, 263.
21 P. K. Robinson, *Essays Biochem.*, 2015, **59**, 1–41.
22 J. A. Bauer, M. Zámocká, J. Majtán and V. Bauerová-Hlinková, *Biomolecules*, 2022, **12**, 472.
23 T. Zhang, Y. Li, W. Hong, Z. Chen, P. Peng, S. Yuan, J. Qu, M. Xiao and L. Xu, *J. Mater. Chem. B*, 2019, **7**, 2190–2200.
24 L.-H. Fu, C. Qi, J. Lin and P. Huang, *Chem. Soc. Rev.*, 2018, **47**, 6454–6472.
25 K. Ashtari, K. Khajeh, J. Fasihi, P. Ashtari, A. Ramazani and H. Vali, *Int. J. Biol. Macromol.*, 2012, **50**, 1063–1069.
26 C. M. Wong, K. H. Wong and X. D. Chen, *Appl. Microbiol. Biotechnol.*, 2008, **78**, 927–938.

27 Q. H. Gibson, B. E. P. Swoboda and V. Massey, *J. Biol. Chem.*, 1964, **239**, 3927–3934.
28 O. A. Khalid, T. S. Claudiu and S. Laurent, *Anti-Cancer Agents Med. Chem.*, 2017, **17**, 164–170.
29 Z. Chen, W. Lu, C. Garcia-Prieto and P. Huang, *J. Bioenerget. Biomembr.*, 2007, **39**, 267–274.
30 M. M. Goyal and A. Basak, *Protein Cell*, 2010, **1**, 888–897.
31 P. Chelikani, I. Fita and P. C. Loewen, *Cell. Mol. Life Sci.*, 2004, **61**, 192–208.
32 L. A. del Río, L. M. Sandalio, J. Palma, P. Bueno and F. J. Corpas, *Free Radic. Biol. Med.*, 1992, **13**, 557–580.
33 A. Rondon, S. Mahri, F. Morales-Yanez, M. Dumoulin and R. Vanbever, *Adv. Funct. Mater.*, 2021, **31**, 2101633.
34 K. Grenda, A. Idström, L. Evenäs, M. Persson, K. Holmberg and R. Bordes, *J. Appl. Polym. Sci.*, 2022, **139**, 51657.
35 L. L. Félix, M. A. Rodriguez Martínez, D. G. Pacheco Salazar and J. A. Huamani Coaquira, *RSC Adv.*, 2020, **10**, 41807–41815.
36 R. Bahulekar, N. R. Ayyangar and S. Ponrathnam, *Enzyme Microb. Technol.*, 1991, **13**, 858–868.
37 M. Arruebo, R. Fernández-Pacheco, M. R. Ibarra and J. Santamaría, *Nano Today*, 2007, **2**, 22–32.
38 M. Moros, B. Pelaz, P. López-Larrubia, M. L. García-Martin, V. Grazú and J. M. de la Fuente, *Nanoscale*, 2010, **2**, 1746–1755.
39 B. Ates, A. Ulu, S. Köytepe, S. A. Ali Noma, V. S. Kolat and T. Izgi, *RSC Adv.*, 2018, **8**, 36063–36075.
40 B. Chen, X. Zhao, Y. Liu, B. Xu and X. Pan, *RSC Adv.*, 2015, **5**, 1398–1405.
41 B. R. Pieters and G. Bardeletti, *Enzyme Microb. Technol.*, 1992, **14**, 361–370.
42 L. M. Rossi, A. D. Quach and Z. Rosenzweig, *Anal. Bioanal. Chem.*, 2004, **380**, 606–613.
43 M. Abbasi, R. Amiri, A.-K. Bordbar, E. Ranjbakhsh and A.-R. Khosropour, *Appl. Surf. Sci.*, 2016, **364**, 752–757.
44 R. Jaquish, A. K. Reilly, B. P. Lawson, E. Golikova, A. M. Sulman, B. D. Stein, N. V. Lakina, O. P. Tkachenko, E. M. Sulman, V. G. Matveeva and L. M. Bronstein, *Int. J. Biol. Macromol.*, 2018, **120**, 896–905.
45 A. G. Rusu, A. P. Chiriac, L. E. Nita, V. Balan, A. M. Serban and A. Croitoriu, *Nanomaterials*, 2022, **12**, 2445.
46 Y. İ. Doğaç and M. Teke, *Preparat. Biochem. Biotechnol.*, 2013, **43**, 750–765.
47 P. Goyal, V. Mishra, I. Dhamija, N. Kumar and S. Kumar, *3 Biotech*, 2022, **12**, 108.
48 R. Massart, *IEEE Trans. Magn.*, 1981, **17**, 1247–1248.
49 M. M. Andersson and R. Hatti-Kaul, *J. Biotechnol.*, 1999, **72**, 21–31.
50 V. Hlady, J. Buijs and H. P. Jennissen, *Methods in Enzymology*, Academic Press, 1999, vol. 309, pp. 402–429.
51 O. P. Murphy, M. Vashishtha, P. Palanisamy and K. V. Kumar, *ACS Omega*, 2023, **8**, 17407–17430.
52 J. J. Virgen-Ortíz, J. C. S. dos Santos, Á. Berenguer-Murcia, O. Barbosa, R. C. Rodrigues and R. Fernandez-Lafuente, *J. Mater. Chem. B*, 2017, **5**, 7461–7490.
53 O. Bozorg-Haddad, M. Delpasand and H. A. Loáiciga, in *Economical, Political, and Social Issues in Water Resources*, ed. O. Bozorg-Haddad, Elsevier, 2021, pp. 217–257.
54 A. Z. Mohammad, J. Sule Suso and N. Forsyth, *Free Radic. Biol. Med.*, 2015, **86**, S16.
55 Y. Li, L. Zhao and X.-F. Li, *Technol. Cancer Res. Treat.*, 2021, **20**, 15330338211036304.
56 J. M. Bolivar, J. Rocha-Martin, C. Mateo, F. Cava, J. Berenguer, R. Fernandez-Lafuente and J. M. Guisan, *Biomacromolecules*, 2009, **10**, 742–747.
57 A. Mosseri, L. Sanchez-Uriel, J. I. Garcia-Peiro, F. Hornos and J. L. Hueso, *Int. J. Mol. Sci.*, 2025, **26**, 5850.
58 O. Barbosa, C. Ortiz, Á. Berenguer-Murcia, R. Torres, R. C. Rodrigues and R. Fernandez-Lafuente, *Biotechnol. Adv.*, 2015, **33**, 435–456.
59 C. S. Sampaio, J. A. F. Angelotti, R. Fernandez-Lafuente and D. B. Hirata, *Int. J. Biol. Macromol.*, 2022, **215**, 434–449.
60 J. Wang, S. Tan, Q. Liang, H. Guan, Q. Han and M. Ding, *Talanta*, 2019, **204**, 792–801.
61 K. Arai, S. Murata, T. Wang, W. Yoshimura, M. Oda-Tokuhisa, T. Matsunaga, D. Kisailus and A. Arakaki, *Journal*, 2022, **23**, 5554.
62 C. Ding, X. Ma, X. Yao and L. Jia, *J. Chromatogr. A*, 2015, **1424**, 18–26.
63 N. M. Eren, G. Narsimhan and O. H. Campanella, *Nanoscale*, 2016, **8**, 3326–3336.
64 N. Hoshyar, S. Gray, H. Han and G. Bao, *Nanomedicine*, 2016, **11**, 673–692.
65 E. J. Tomotani and M. Vitolo, *Enzyme Microb. Technol.*, 2007, **40**, 1020–1025.
66 B. Kranz, J. Bürck, M. Franzreb, R. Köster and A. S. Ulrich, *J. Colloid Interface Sci.*, 2007, **316**, 413–419.
67 R. M. Abdallah and R. M. S. Al-Haddad, *J. Nano Res.*, 2022, **74**, 59–68.
68 J. Yu, L. Yang, X. Liang, T. Dong and H. Liu, *Analyst*, 2015, **140**, 4114–4120.
69 J. R. Casey, S. Grinstein and J. Orlowski, *Nat. Rev. Mol. Cell Biol.*, 2010, **11**, 50–61.
70 M. P. Calatayud, B. Sanz, V. Raffa, C. Riggio, M. R. Ibarra and G. F. Goya, *Biomaterials*, 2014, **35**, 6389–6399.
71 J. Bai, H. Ma, X. Fan, H. Yang, C. Liu, Z. Xu and Y. Liu, *Res. Mater.*, 2022, **14**, 100267.
72 P. T. A. Santos, P. M. A. G. Araújo, E. Leal, I. L. T. de Albuquerque, L. S. Conrado and A. C. F. d M. Costa, *Mater. Sci. Forum*, 2015, **820**, 161–166.
73 G. Ozyilmaz, S. S. Tukel and O. Alptekin, *J. Mol. Catal. B: Enzym.*, 2005, **35**, 154–160.
74 A. G. Rusu, A. P. Chiriac, L. E. Nita, V. Balan, A. M. Serban and A. Croitoriu, *Nanomaterials*, 2022, **12**(14), 2445.
75 Ö. Alptekin, S. Seyhan Tükel, D. Yildirim and D. Alagöz, *Enzyme Microb. Technol.*, 2011, **49**, 547–554.
76 J. Ran, S. Jia, Y. Liu, W. Zhang, S. Wu and X. Pan, *Bioresour. Technol.*, 2010, **101**, 6285–6290.
77 D. Yang, X. Wang, J. Shi, X. Wang, S. Zhang, P. Han and Z. Jiang, *Biochem. Eng. J.*, 2016, **105**, 273–280.
78 R. Yavaşer and A. A. Karagözler, *Appl. Biochem. Biotechnol.*, 2020, **192**, 1191–1206.
79 J. Shentu, J. Wu, W. Song and Z. Jia, *Int. J. Biol. Macromol.*, 2005, **37**, 42–46.

